

Fault Tolerant Robust Flight Control Using Surface Actuator Hinge Moments

Ryan T. Ratliff
The Boeing Company
St. Louis, MO, USA
ryan.t.ratliff@boeing.com

Prabhakar R. Pagilla
Mechanical and Aerospace Engineering
Oklahoma State University
Stillwater, OK, USA
pagilla@okstate.edu

Abstract—A robust, flight control law is investigated to provide fault tolerance for air vehicles experiencing inertial state measurement sensor degradation. The method is particularly useful on low cost, precision weapons pursuing dynamic targets. Observation techniques are facilitated by representing the surface actuator aerodynamic induced hinge moment by a function that is Lipschitz within the actuator sweep angle. A stable output feedback flight control law, requiring only actuator angular position and current measurements, is designed to handle the hinge moment effects and track a predetermined angle-of-attack reference trajectory. Benefits include improved effectiveness, improved reliability without additional hardware, and a cost and weight savings. Simulations are conducted on a tactical missile interceptor to evaluate the controller at various operating conditions in the flight envelope.

I. INTRODUCTION

As war zones transition to large cities and urban areas, it is becoming necessary to consider civilian populations when selecting battlefield weapons. Therefore, modern tactical munitions are becoming smaller and more numerous in a given battlespace. With recent developments in modern guidance systems, minaturization of these weapons allows increased precision while reducing the risk of collateral damage. However, attacking and/or defending against specific targets encompassing large civilian areas can require large numbers of offensive and defensive munitions with unprecedented accuracy. The risk of system failures invariably will increase with the number of active weapons in the battlespace. It is desirable to keep system costs low and many of these weapons will guide and control autonomously without a contingency management protocol subsequent to launch.

Most air vehicles possess an inertial measurement unit (IMU) to measure the respective airframe rates and accelerations. These measurements are subsequently fed back to the guidance and flight control computer for processing. The following study specifically addresses issues associated with corruption or loss of IMU sensor feedback. This could result from noise corruption, saturation caused by high accelerations during a boost phase, or complete sensor failure. Degredation or loss of IMU sensor integrity in a tactical precision munition would seriously inhibit flight control system response to guidance commands. Cumulative errors result in a missed target intercept and effectively

introduce an unguided munition in a potentially civilian populated battlespace.

For this study, it is desired to provide an alternative to inertial measurements during a faulted state by using an observer. The observer relies on the actuator dynamics along with the nonlinear hinge moment induced by aerodynamic forces on the actuator surfaces. Research on nonlinear observers is extensive in the literature. Observers for nonlinearities satisfying a Lipschitz condition are considered in [1]. A special form of the observer in [1] with a state feedback regulation controller is developed in [2] and shown to satisfy certainty equivalence.

In this research, it is required that the air vehicle track a predetermined angle-of-attack (AoA) reference trajectory. Following from [2], a solution to the output feedback tracking control problem is expounded. A dynamic model augmented with aerodynamic hinge moment bias from the flight control surface actuator is provided. Aerodynamic hinge moments are estimated using computational fluid dynamics (CFD) and modeled as a nonlinear, multivariable continuous function. The hinge moment bias contribution is shown to be locally Lipschitz within the actuator sweep angle for specified flight conditions. The overall system model is presented as separate linear and nonlinear components. A linear, full-state feedback controller is designed with a sufficient condition under which exponential stabilization is achieved. With only actuator position and current output available for measurement, a nonlinear observer is designed and a sufficient condition developed for exponential stability. Based on the controller and observer design, certainty equivalence is obtained and simulations are conducted on a tactical missile interceptor to verify flight control law performance.

II. MODELING

Although many guided munitions use IMU measurements to predict inertial velocity, the modeling effort in this section assumes that the weapon velocity components can be acquired from an external tracking source such as a fire control radar. Future work, discussed in Section VI, will investigate the feasibility of augmenting the dynamics with a true velocity state.

Neglecting gravity, for a given airspeed and altitude, the nonlinear, longitudinal equations of motion can be described

by [3]

$$m\dot{\alpha}V_T = F_T \sin \alpha - L_A(\alpha, \delta) + mV_T q \quad (1)$$

$$\dot{q} = \frac{M(\alpha, \delta)}{I_{yy}} \quad (2)$$

where F_T is the propulsion force, α is the angle-of-attack and q is the pitch rate. The aerodynamic lift force, L_A , and pitching moment, M , are functions of α and actuator control surface angular deflection, δ . The constants V_T , m , and I_{yy} represent the vehicle airspeed, mass, and pitch axis moment of inertia, respectively. For this study, the propulsion forces are assumed to be zero and changes in the lift force and pitching moment are relatively linear within the flight envelope and can be linearized to give

$$\dot{\alpha} = \frac{Z_\alpha}{V_T} \alpha + \frac{Z_\delta}{V_T} \delta + q \quad (3)$$

$$\dot{q} = M_\alpha \alpha + M_\delta \delta \quad (4)$$

where $Z_{(\bullet)}$, $M_{(\bullet)}$ are the corresponding acceleration and moment stability derivative constants relative to (\bullet) , respectively.

For most vehicles, δ is considered a “virtual” deflection and is resolved from an internal surface mixing strategy that incorporates multiple true fin deflections. To facilitate this preliminary study, a vehicle was designed where virtual deflections and true deflections map one-to-one. The true control surface deflection is typically measured relative to the vehicle body axis coordinate system. Figure 1 illustrates this convention and depicts the influence of an aerodynamic drag force, F_D , inducing an actuator hinge moment. The resulting hinge moment bias, M_H , is nonlinear and a combined torque profile can be represented as a multi-variable, continuous, scalar function which can be deduced mathematically from Figure 1 as

$$M_H = F_D l_H \sin(\delta - \alpha) = \frac{1}{2} \rho V_T^2 S_H l_H \sin(\delta - \alpha) \quad (5)$$

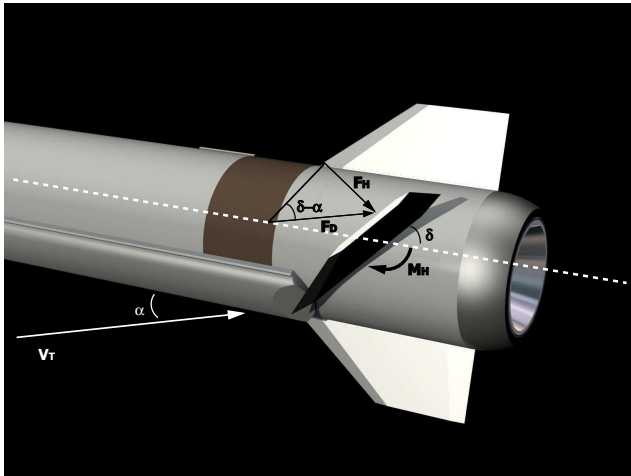


Fig. 1. Aerodynamic hinge moment bias description

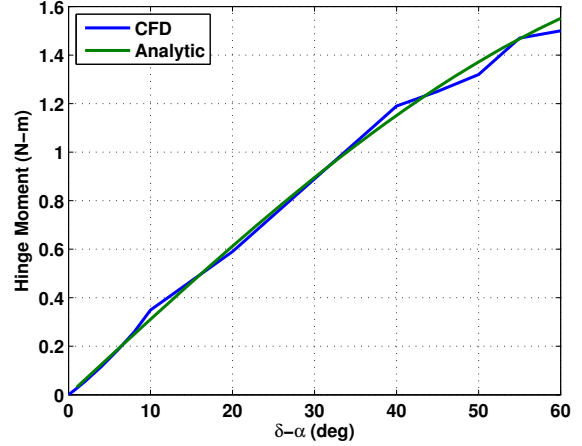


Fig. 2. Aerodynamic hinge moment bias comparison

where ρ is the air density, and l_H , S_H are an aerodynamic reference length and area, respectively. Figure 2 shows the hinge moment computed using equation (5) compared to a CFD approximation. More complex geometries will invariably produce more complex airflows. Therefore, the relationship in (5) will not necessarily hold for all configurations. Other methods such as polynomial curve-fitting or piece-wise approximations may be required. The subsequent control design discussed in Section III, however, can still be applied. The flight control surface on most small, low cost munitions is electro-mechanically actuated and can be modeled as a linear DC motor. The nonlinear hinge moment bias component enters as an external disturbance. Assigning a convention where the hinge moment bias opposes the internal actuator torque when positive current is applied, the mechanical dynamics of the flight control actuator can be represented as

$$J\ddot{\delta} = K_t i - M_H(\alpha, \delta) \quad (6)$$

where i is the applied current and J and K_t are the system inertia and motor torque constant, respectively. The electrical circuit dynamics of the actuator are described by

$$V_s = Ri + L \frac{di}{dt} + V_b \quad (7)$$

where R and L are the coil resistance and inductance, respectively, $V_b = K_t \dot{\delta}$ is the back electro-motive force, and V_s is the supply voltage control input signal. Combining equations (3)-(7) and choosing the states as $[\alpha \ q \ \delta \ \dot{\delta} \ i] = [x_1 \ x_2 \ x_3 \ x_4 \ x_5]$ gives the state-space representation

$$\begin{aligned} \dot{x}_1 &= \mu_1 x_1 + x_2 + \mu_2 x_3 \\ \dot{x}_2 &= M_\alpha x_1 + M_\delta x_3 \\ \dot{x}_3 &= x_4 \\ \dot{x}_4 &= \mu_3 [K_t x_5 - M_H(x_1, x_3)] \\ \dot{x}_5 &= \mu_4 (-K_t x_4 - R x_5 + u) \end{aligned} \quad (8)$$

where

$$\mu_1 = \frac{Z_\alpha}{V_T}, \mu_2 = \frac{Z_\delta}{V_T}, \mu_3 = \frac{1}{J}, \mu_4 = \frac{1}{L}$$

Angle-of-attack is typically computed from inertial measurement quantities and, subsequently fed back to the flight control algorithm for tracking error computation. However, lacking a valid measurement of inertial quantities, only the surface actuator position and current are considered legitimate outputs

$$y_1 = x_3, \quad y_2 = x_5 \quad (9)$$

Although a global representation of the hinge moment bias is not required, the anticipated flight conditions could conceivably result in the quantity $(\delta - \alpha) > \frac{\pi}{6}$. Therefore, a linear approximation would be insufficient. Including the second term in an infinite series approximation of $\sin(\delta - \alpha)$ and defining $\mu_H = \frac{1}{2}\rho V_T^2 S_H l_H$ from (5) gives

$$\hat{M}_H = \mu_H \left[(\delta - \alpha) - \frac{1}{6}(\delta - \alpha)^3 \right] \quad (10)$$

By redefining the hinge moment bias as

$$\psi = \hat{M}_H - \mu_H(\delta - \alpha) \quad (11)$$

equation (8) can be rewritten as

$$\begin{aligned} \dot{x} &= Ax + Bu + \Psi \\ y &= Cx \end{aligned} \quad (12)$$

where

$$A = \begin{bmatrix} \mu_1 & 1 & \mu_2 & 0 & 0 \\ M_\alpha & 0 & M_\delta & 0 & 0 \\ 0 & 0 & 0 & 1 & 0 \\ \mu_3 \mu_H & 0 & -\mu_3 \mu_H & 0 & \mu_3 K_t \\ 0 & 0 & 0 & -\mu_4 K_t & -\mu_4 R \end{bmatrix}$$

$$B^T = [0 \ 0 \ 0 \ 0 \ \mu_4] \quad B_\psi^T = [0 \ 0 \ 0 \ -\frac{\mu_3 \mu_H}{6} \ 0]$$

$$C = \begin{bmatrix} 0 & 0 & 1 & 0 & 0 \\ 0 & 0 & 0 & 0 & 1 \end{bmatrix}$$

and

$$\Psi(x) = B_\psi(x_3 - x_1)^3 \quad (13)$$

Let $\Delta_{\max} = \|\delta - \alpha\|_\infty$. For a given airspeed and altitude, the nonlinearity, Ψ , is locally Lipschitz, with constant γ , within the set of all possible AoA and actuator angular positions of the flight envelope

$$\|\Psi(x_a) - \Psi(x_b)\| \leq \gamma \|x_a - x_b\| \quad (14)$$

$$\forall x_a, x_b \in X \quad X := \{x \in \mathbb{R}^5 \mid 0 \leq |x_3 - x_1| \leq \Delta_{\max}\}$$

III. OUTPUT FEEDBACK CONTROL DESIGN

A controller is necessary to track a predetermined AoA reference trajectory. The predetermined reference trajectory, x_r , can be selected to satisfy a reference model with a desired dynamic performance corresponding to

$$\dot{x}_r = Ax_r + Bu_r + \Psi(x_r) \quad (15)$$

Although it is necessary to track AoA and pitch rate, the output vector from (12) only provides actuator position and current measurement. Therefore, an output feedback tracking controller is required. This section outlines the development of a stable, output feedback controller with a nonlinear observer beginning with the following definition:

Definition 1: [4] Suppose $\mathcal{A} \in \mathbb{C}^{n \times n}$ is stable in the sense that all eigenvalues have negative real parts. Then

$$\delta_s(\mathcal{A}) = \min_{\omega \in \mathbb{R}} \sigma_{\min}(\mathcal{A} - j\omega I) \quad (16)$$

is the distance to the set of unstable matrices where $\sigma_{\min}(\mathcal{A} - j\omega I)$ is the minimum singular value of $(\mathcal{A} - j\omega I)$, $\forall \omega \in \mathbb{R}$.

Lemma 1: Consider the Algebraic Riccati Equation (ARE)

$$\mathcal{A}^*P + P\mathcal{A} + PP + \rho I = 0$$

and associated Hamiltonian matrix

$$\mathbb{H} = \begin{bmatrix} \mathcal{A} & I \\ -\rho I & -\mathcal{A}^* \end{bmatrix}$$

where $\rho > 0$ and \mathcal{A} is Hurwitz. If $\sqrt{\rho} < \delta_s(\mathcal{A})$, then \mathbb{H} is hyperbolic (all eigenvalues of \mathbb{H} have nonzero real parts) and there exists a unique $P = P^T > 0$ which is the solution to the ARE.

Proof: The eigenvalues of \mathbb{H} may be found by considering

$$\begin{aligned} \det(sI - \mathbb{H}) &= \det \begin{bmatrix} sI - \mathcal{A} & -I \\ \rho I & sI + \mathcal{A}^* \end{bmatrix} \\ &= \det[(sI - \mathcal{A})(sI + \mathcal{A}^*) + \rho I] = 0 \end{aligned}$$

It follows that $s = j\omega$ is an eigenvalue of \mathbb{H} if the matrix

$$[(\mathcal{A} - j\omega I)^*(\mathcal{A} - j\omega I) - \rho I]$$

is singular. Noting from (16) that $\delta_s^2(\mathcal{A})I \leq (\mathcal{A} - j\omega I)^*(\mathcal{A} - j\omega I)$, the eigenvalues of \mathbb{H} will always have nonzero real parts if $\delta_s^2(\mathcal{A}) - \rho > 0$ or $\sqrt{\rho} < \delta_s(\mathcal{A})$. ■

In order to fulfill the AoA tracking requirement and manage the hinge moment nonlinearity outlined in Section II, an output feedback controller consisting of a linear state feedback control law coupled with a nonlinear observer is presented.

Theorem 1: Consider the system given by (12) with nonlinearity defined by (14). The output tracking control law

$$u = L\hat{x}_{5r} + Rx_{5r} + K_t x_{4r} - K_c \hat{e} \quad (17)$$

with $\hat{e} = \hat{x} - x_r$ and nonlinear observer

$$\dot{\hat{x}} = A\hat{x} + Bu + \Psi(\hat{x}) + \mathcal{L}_o(y - C\hat{x}) \quad (18)$$

where $\mathcal{K}_c, \mathcal{L}_o \in \mathbb{R}^5$ are gain vectors chosen such that $A_c = A - B\mathcal{K}_c$ and $A_o = A - \mathcal{L}_oC$ are Hurwitz, renders the tracking error dynamics

$$\dot{e} = A_c e + \Psi(x) - \Psi(x_r), \quad e = x - x_r \quad (19)$$

and observer error dynamics

$$\dot{\tilde{x}} = A_o \tilde{x} + \Psi(x) - \Psi(\hat{x}), \quad \tilde{x} = x - \hat{x} \quad (20)$$

exponentially stable for all $x \in X$ if

$$\gamma < \delta_s(A_c) \quad \text{and} \quad \gamma < \delta_s(A_o) \quad (21)$$

Proof: Substituting (17) into (8) gives

$$\dot{e} = A_c e + B_c \mathcal{K}_c \tilde{x} + \Psi(x) - \Psi(x_r) \quad (22)$$

Consider a Lyapunov function candidate

$$V(e, \tilde{x}) = \xi e^T P_c e + \tilde{x}^T P_o \tilde{x} \quad (23)$$

where ξ is a positive constant and $P_c, P_o \in \mathbb{R}^{5 \times 5}$ are symmetric, positive definite. Taking the time derivative of (23) yields

$$\begin{aligned} \dot{V}(e, \tilde{x}) &= \xi \{ e^T (A_c^T P_c + P_c A_c) e + 2e^T P_c [\Psi(x) - \Psi(x_r)] + \\ &2e^T P_c B_c \mathcal{K}_c \tilde{x} \} + \tilde{x}^T [A_o^T P_o + P_o A_o] \tilde{x} + 2\tilde{x}^T P_o [\Psi(x) - \Psi(\hat{x})] \\ &\leq \xi \{ e^T (A_c^T P_c + P_c A_c) e + 2\gamma \|P_c e\| \|e\| + 2P_c B_c \mathcal{K}_c \|e\| \|\tilde{x}\| \} \\ &\quad + \tilde{x}^T (A_o^T P_o + P_o A_o) \tilde{x} + 2\gamma \|P_o \tilde{x}\| \|\tilde{x}\| \\ &\leq \xi \{ e^T (A_c^T P_c + P_c A_c + P_c P_c + \gamma^2 I) e + 2P_c B_c \mathcal{K}_c \|e\| \|\tilde{x}\| \} \\ &\quad + \tilde{x}^T (A_o^T P_o + P_o A_o + P_o P_o + \gamma^2 I) \tilde{x} \end{aligned}$$

Now, for any $\eta_c, \eta_o > 0$, there exist symmetric, positive definite P_c, P_o such that

$$A_c^T P_c + P_c A_c + P_c P_c + \gamma^2 I = -\eta_c I \quad (24)$$

$$A_o^T P_o + P_o A_o + P_o P_o + \gamma^2 I = -\eta_o I \quad (25)$$

if the associated Hamiltonian matrices

$$\mathbb{H}_c = \begin{bmatrix} A_c & I \\ -(\gamma^2 + \eta_c)I & -A_c^T \end{bmatrix}, \quad \mathbb{H}_o = \begin{bmatrix} A_o & I \\ -(\gamma^2 + \eta_o)I & -A_o^T \end{bmatrix}$$

are hyperbolic. From (21) in the hypothesis, consider the continuous function $f(\gamma) = \gamma^2 - \delta_s^2(A_c) < 0$. Since f is continuous, there exists $\eta_c > 0$ such that

$$f(\gamma) = \gamma^2 + \eta_c - \delta_s^2(A_c) < 0 \quad \text{or} \quad \sqrt{\gamma^2 + \eta_c} < \delta_s(A_c)$$

A similar continuity argument can be made regarding the observer resulting in $\sqrt{\gamma^2 + \eta_o} < \delta_s(A_o)$. Therefore, the Hamiltonian matrices, \mathbb{H}_c and \mathbb{H}_o , are hyperbolic from Lemma 1, and it follows from (24) and (25) that

$$\dot{V}(e, \tilde{x}) \leq -\xi \eta_c \|e\|^2 + 2\xi P_c B_c \mathcal{K}_c \|e\| \|\tilde{x}\| - \eta_o \|\tilde{x}\|^2 \quad (26)$$

Defining $\xi_c = 2\|P_c B_c \mathcal{K}_c\|, \xi = \frac{\eta_c \eta_o}{\xi_c^2}$, and noting

$$\left(\frac{1}{\sqrt{2}} \frac{\eta_c \sqrt{\eta_o}}{\xi_c} \|e\| - \frac{1}{\sqrt{2}} \sqrt{\eta_o} \|\tilde{x}\| \right)^2 \geq 0 \quad (27)$$

gives

$$\begin{aligned} \dot{V}(e, \tilde{x}) &\leq -\xi \eta_c \|e\|^2 + \xi \xi_c \|e\| \|\tilde{x}\| - \eta_o \|\tilde{x}\|^2 \\ &\leq -\frac{\eta_c^2 \eta_o}{\xi_c^2} \|e\|^2 + \frac{\eta_c \eta_o}{\xi_c} \|e\| \|\tilde{x}\| - \eta_o \|\tilde{x}\|^2 \\ &\leq -\frac{1}{2} \left(\frac{\eta_c^2 \eta_o}{\xi_c^2} \|e\|^2 + \eta_o \|\tilde{x}\|^2 \right) \end{aligned} \quad (28)$$

Therefore, $V(e, \tilde{x})$ is a Lyapunov function and $e, \tilde{x} \rightarrow 0$ exponentially as $t \rightarrow \infty$. ■

Remark 1: The number δ_s is realization dependent. Therefore, a coordinate transformation, $x' = Tx$, can be used to reduce the value of γ and increase δ_s [5]. When using standard SI units, the actuator inertia is typically very small relative to K_t, R , and L resulting in large values of μ_3 . A similarity transformation $e' = Te$ where

$$\|T^{-1}\psi(Tx_a) - T^{-1}\psi(Tx_b)\| \leq \gamma' \|x_a - x_b\| \quad (29)$$

can be used to produce a new Lipschitz constant where $\gamma' < \gamma$.

IV. TRAJECTORY GENERATION

Full-state reference trajectories must be provided to the controller of Section III for tracking. For output α , the relative degree of the full state system (8) is four and, therefore, four differentiations of the output are required to compute a desired feedforward reference trajectory. For a given set of desired initial and final boundary conditions on α , a polynomial interpolation method [6] was used to produce smooth, continuous trajectories in α and corresponding derivatives. Given the desired initial and final values of α , an equilibrium could be calculated using (4) to determine the initial and final values of δ required to trim the vehicle. The actuator deflection trajectory dynamics can then be computed from

$$\mu_2 \dot{\delta} = -M_\delta \delta + \ddot{\alpha} - \mu_1 \dot{\alpha} - M_\alpha \alpha \quad (30)$$

Once the differential equation (30) is solved for δ , the remaining derivatives $\dot{\delta}, \ddot{\delta}, \ddot{\alpha}$ can be found analytically by two more differentiations of (30) and using $\ddot{\alpha}, \alpha^{(4)}$. Now that all derivatives in α and δ are known, q and i can be determined from (3) and (6), respectively. Differentiating (6), solving for di/dt , and substituting into (7) results in the feedforward control voltage reference

$$\begin{aligned} V_s^{ff} &= \mu_H K_t L [\cos(\delta - \alpha)(1 - \alpha)\dot{\delta} \\ &\quad + \cos(\delta - \alpha)(\delta - 1)\dot{\alpha} + \ddot{\delta}] + K_i \dot{\delta} + R i \end{aligned} \quad (31)$$

This particular strategy, as described here, is capable of being discretized and solved in real-time.

V. SIMULATION RESULTS

Simulations were conducted to verify the control design developed in the previous section. To reflect the performance of a small, agile precision weapon, it was desired that the airframe perform a 10° α -maneuver in 100 milliseconds at Mach 3. Values for the airframe and actuator

TABLE I
AIRFRAME PARAMETERS

Parameter	Value
Z_α ($\frac{m}{\text{sec}^2 \text{-rad}}$)	-3250
Z_δ ($\frac{m}{\text{sec}^2 \text{-rad}}$)	475
M_α ($\frac{1}{\text{sec}^2}$)	-4481
M_δ ($\frac{1}{\text{sec}^2}$)	5186
V_T ($\frac{m}{\text{sec}}$)	1018

TABLE II
ACTUATOR PARAMETERS

Parameter	Value
K_t ($\frac{N \cdot m}{\text{amp}}$)	0.562
J ($\text{kg} \cdot \text{m}^2$)	0.005
R (Ω)	1.420
L (mH)	10
V_{max} (Volt)	48
S_H (cm^2)	14.0
l_H (cm)	0.140

parameters are given in Tables I and II, respectively. The predetermined state reference trajectories were computed using the algorithm discussed in Section IV.

The Lipschitz constant was determined from (14) and the maximum value of $\delta - \alpha$. Based on the maneuverability requirements of the munition, AoA would not exceed a range of $\pm 25^\circ$. The operational limits for actuator deflection were $\pm 35^\circ$. Therefore, $\Delta_{\text{max}} = \frac{\pi}{3} \text{rad}$. Simple differentiation of Ψ , as given in (13), shows that a maximum occurs at $\delta - \alpha = \frac{\pi}{3}$ and results in a Lipschitz constant, $\gamma = 426$.

The control gains to produce A_c were initially selected such that the time constant on α was at least three times that of the desired maneuver time. The observer poles were selected to be five times faster than the controller poles. Note from Table II that the value of the actuator inertia in SI units was small compared to the other physical parameters in the system resulting in a large quantity $\mu_3 \mu_H$ which directly affects the nonlinearity (13). Therefore, a transformation, as discussed in Remark 1, was required to reduce the Lipschitz constant.

Excessive overshoot was noted on the actuator deflection and in several cases the control effort was close to saturation. Therefore, the gains were adjusted accordingly to mitigate these effects. Final values of the control gains and observer gains were determined as

$$\mathcal{K}_c = [-688 \ 104 \ 674 \ 36 \ 9]$$

$$L_o^T = \begin{bmatrix} -8 & -197 & -1 & -48 & 7 \\ -228 & -1069 & 2 & -96 & 8 \end{bmatrix} \quad (32)$$

The transformations selected to reduce the Lipschitz constant and meet the sufficient condition of Theorem 1 were

$$T_c = \text{diag}\{1 \ 1 \ 1 \ 1000 \ 1\} \rightarrow e' = T_c e$$

$$T_o = \text{diag}\{1 \ 1 \ 1 \ 2000 \ 1\} \rightarrow \tilde{x}' = T_o \tilde{x}$$

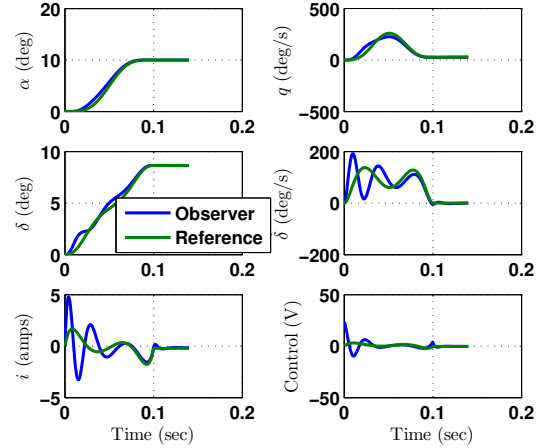


Fig. 3. Trajectory comparison, 10° maneuver

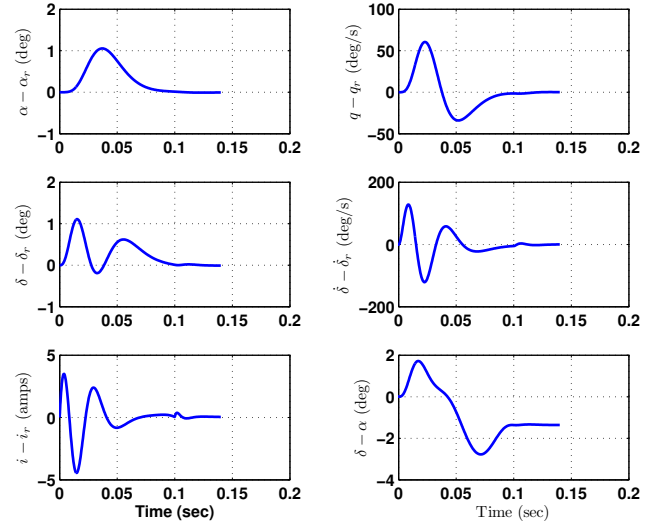


Fig. 4. State trajectory error 10° maneuver

The corresponding Lipschitz constants and distance to singularity were computed as

$$\sqrt{(\gamma'_c)^2 + \eta_c} = 0.48 < \delta_s(A_c) = 0.49$$

$$\sqrt{(\gamma'_o)^2 + \eta_o} = 0.38 < \delta_s(A_o) = 0.98$$

where $\eta_c = 0.05$ and $\eta_o = 0.1$. Figure 3 compares the observed and reference trajectories of a 10° maneuver where the observer initial condition $\hat{\alpha}$ was set to 2° . The controller immediately begins to compensate for the observer discrepancy which produces large transient errors in the actuator rate dynamics. This transient is also reflected in the true state tracking error shown in Figure 4. As the observer converges (Fig. 5), the errors are mitigated and exponential tracking behavior is exhibited. To evaluate the limits of the control law, the observer initial condition was set at $\hat{\alpha} = -30^\circ$ and $\hat{\delta} = 9^\circ$ for a maneuver transferring α from $10^\circ \rightarrow -5^\circ$ in 500 milliseconds. In this case, the *observed* hinge moment nonlinearity was initially more than twice

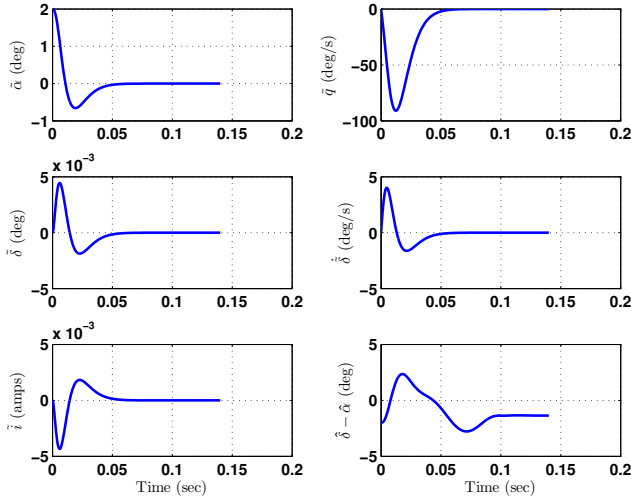


Fig. 5. Observer error 10° maneuver

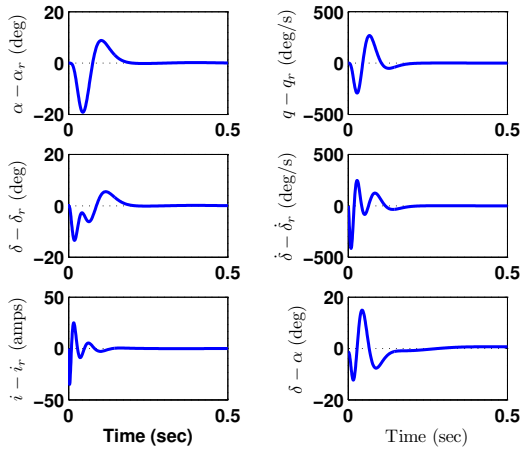


Fig. 6. State trajectory error 15° maneuver

that of the actual value. Although the observer converges quickly, a maximum error of 20° is exhibited between the α state and reference trajectory prior to convergence at around 300 milliseconds. Actuator control power is close to saturation and the actuator deflection rates are approaching feasible limits. Tracking and observer performance for the 15° α -maneuver are shown in Figures 6 and 7, respectively.

VI. CONCLUSION

The research presented a preliminary study on feasibility of an output feedback tracking control law with application to flight control of air vehicles. The control law compensates for absence of airframe inertial state information. Application to guided air munitions is of particular interest. The architecture requires knowledge of the behavior and bounds on the surface control actuator hinge moments relative to flight condition. It is shown that this behavior can be represented by functions that are Lipschitz within the

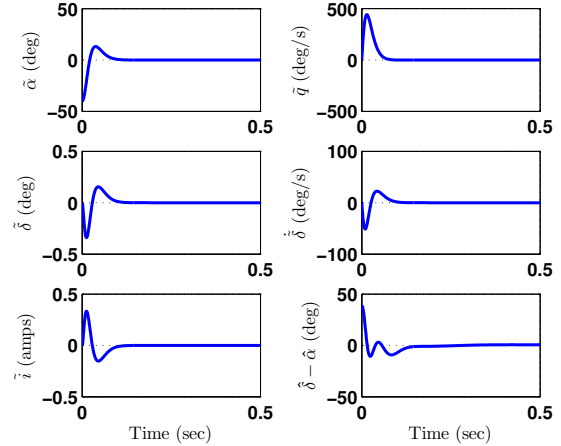


Fig. 7. Observer error 15° maneuver

actuator state-space. An exponentially stable tracking controller, using only actuator position and current feedback, was developed to track a predetermined reference trajectory and handle the nonlinear effects. Controller performance was evaluated with simulation analysis and robustness was demonstrated by varying the observer initial conditions. The closed-loop actuator dynamics exhibited sensitivity to large observation errors as a result of large actuator/airframe time constant separation.

Various airframe and surface configurations will ultimately be encountered. Therefore, future work will focus on alternative hinge moment approximation methods to address multiple and potentially time-varying configurations. Additionally, fin mixing strategies will need to be incorporated into the design architecture. Further investigations are also required in reference trajectory designs to address implementation and performance issues. Designs which incorporate airspeed and propulsion dynamics need to be evaluated along with feasibility of a gain scheduling architecture. Alternate methods will also be investigated to address parameter variation and modeling uncertainty.

REFERENCES

- [1] C. Aboky, G. Sallet, and J. Vivalda, "Observers for Lipschitz nonlinear systems," *International Journal of Control*, vol. 75, no. 3, pp. 204–212, 2002.
- [2] P. R. Pagilla and Y. Zhu, "Controller and observer design for Lipschitz nonlinear systems." Proceedings IEEE American Control Conference, July 2004.
- [3] B. L. Stevens and F. L. Lewis, *Aircraft Control and Simulation*, 2nd ed. New Jersey: John Wiley and Sons, 2003.
- [4] R. Byers, "A bisection method for measuring the distance of a stable matrix to the unstable matrices," *SIAM Journal of Scientific and Statistical Computing*, vol. 9, pp. 875–881, 1988.
- [5] R. Rajamani and Y. M. Cho, "Existence and design of observers for nonlinear systems: Relation to distance to unobservability," *International Journal of Control*, vol. 69, no. 5, pp. 717–731, 1998.
- [6] M. W. Spong and M. Vidyasagar, *Robot Dynamics and Control*. New York: John Wiley and Sons, 1989.